10-5-2000

Chandra X-Ray Observations of the Hydra A Cluster: An Interaction between the Radio Source and the X-Ray–emitting Gas

B. R. McNamara
Harvard-Smithsonian Center for Astrophysics

M. Wise
Massachusetts Institute of Technology

P. Nulsen
University of Wollongong

L. P. David
Harvard-Smithsonian Center for Astrophysics

C. L. Sarazin
University of Virginia

See next page for additional authors

THE ASTROPHYSICAL JOURNAL, 534:L135–L138, 2000 May 10

CHANDRA X-RAY OBSERVATIONS OF THE HYDRA A CLUSTER: AN INTERACTION BETWEEN THE RADIO SOURCE AND THE X-RAY–EMITTING GAS

B. R. MCNAMARA,[1] M. WISE,[2] P. E. J. NULSEN,[1,3] L. P. DAVID,[1] C. L. SARAZIN,[4] M. BAUTZ,[2]
M. MARKEVITCH,[1] A. VIKHLININ,[1] W. R. FORMAN,[1] C. JONES,[1] AND D. E. HARRIS,[1]
Received 2000 January 24; accepted 2000 March 17; published 2000 May 5

ABSTRACT

We present *Chandra* X-ray observations of the Hydra A cluster of galaxies, and we report the discovery of structure in the central 80 kpc of the cluster's X-ray–emitting gas. The most remarkable structures are depressions in the X-ray surface brightness, ~25–35 kpc in diameter, that are coincident with Hydra A's radio lobes. The depressions are nearly devoid of X-ray–emitting gas, and there is no evidence for shock-heated gas surrounding the radio lobes. We suggest that the gas within the surface brightness depressions was displaced as the radio lobes expanded subsonically, leaving cavities in the hot atmosphere. The gas temperature declines from 4 keV at 70 kpc to 3 keV in the inner 20 kpc of the brightest cluster galaxy (BCG), and the cooling time of the gas is ~600 Myr in the inner 10 kpc. These properties are consistent with the presence of an ~34 $M_\odot$ yr^{-1} cooling flow within a 70 kpc radius. Bright X-ray emission is present in the BCG surrounding a recently accreted disk of nebular emission and young stars. The star formation rate is commensurate with the cooling rate of the hot gas within the volume of the disk, although the sink for the material that may be cooling at larger radii remains elusive. A bright, unresolved X-ray source is present in the BCG's nucleus, coincident with the radio core. Its X-ray spectrum is consistent with a power law absorbed by a foreground $N_{\rm H} \simeq 4 \times 10^{22}$ cm^{-2} column of hydrogen. This column is roughly consistent with the hydrogen column seen in absorption toward the $\lesssim$24 pc diameter VLBA radio source. Apart from the point source, no evidence for excess X-ray absorption above the Galactic column is found.

Subject headings: cooling flows — galaxies: clusters: individual (Hydra A)

1. INTRODUCTION

The Hydra A radio galaxy is associated with a relatively poor cluster of galaxies at redshift $z = 0.052$. The cluster harbors an atmosphere of X-ray–emitting gas of luminosity $L_{\rm X}(0.5–4.5) = 2.2 \times 10^{44}$ ergs s^{-1} and a mean gas temperature of ~4 keV based on *Einstein* MPC observations (David et al. 1990) and *ASCA* observations (Ikebe et al. 1997). A cooling flow is present with an accretion rate of $\dot{M} \sim 250\ M_\odot$ yr^{-1} (assuming $H_0 = 50$ km s^{-1} Mpc^{-1}) within a radius of $\simeq$170 kpc (White, Jones, & Forman 1997; Peres et al. 1998). The hot atmosphere is centered on the brightest cluster elliptical galaxy (BCG) that hosts the large (80″ or 84 kpc in projection), unusually powerful ($P = 1.6 \times 10^{26}$ W Hz^{-1} at 178 MHz) Fanaroff-Riley type 1 radio source 3C 218 (Ekers & Simkin 1983; Taylor et al. 1990; Taylor 1996). The twin jet-lobe radio source emerges from a disk of young stars (McNamara 1995; Hansen, Jørgenson, & Nørgaard-Nielson 1995; Melnick, Gopal-Krishna, & Terlevich 1997) and nebular emission (Ekers & Simkin 1983; Hansen et al. 1995; Baum et al. 1988) several kiloparsecs in size that is in rotation about the nucleus. H I is seen in absorption toward the nucleus (Dwarakanath, Owen, & van Gorkom 1995) and has been mapped in absorption against the parsec-scale nuclear radio source with the VLBA (Taylor 1996).

Hydra A was observed by the *Chandra X-Ray Observatory* during its orbital verification and activation phase. Hydra A's several interesting properties provide a first opportunity to investigate the cooling flow and the potential interactions between the radio source and the X-ray–emitting gas using *Chandra*'s unprecedentedly high spatial resolution. We present an analysis of Hydra A based on the preliminary telescope calibration in this Letter, and we report the discovery of an interaction between the radio source and the X-ray–emitting gas. We assume $H_0 = 70$ km s^{-1} Mpc^{-1}, $\Omega_M = 0.3$, $\Omega_\Lambda = 0.7$, a luminosity distance of 240 Mpc, and 1″ = 1.05 kpc.

2. DATA ANALYSIS

The calibration observations of Hydra A were performed on 1999 October 30. A total integration time of 40 ks was obtained, 20 ks centered at the aim point of the S3 back-illuminated Advanced CCD Imaging Spectrometer (ACIS) chip (observation 576) and 20 ks centered at the ACIS-I aim point on the I3 front-illuminated device (observation 575). X-ray events with energies below 300 eV and above 10 keV were not considered in our analysis, and flight grades 0, 2, 3, 4, and 6 were retained. The particle background was generally stable throughout the S3 observations. Only 300 s of the 20 ks exposure experienced a 30% increase in particle background. Therefore, no S3 data were rejected on this basis. The spectral analysis presented here is limited to a 0.5–7 keV bandpass for the S3 data. Data obtained with the imaging array were excluded from the spectral analysis.

2.1. *X-Ray Morphology*

A *Chandra* image of the X-ray emission from the central 118″ × 118″ of the cluster is shown in Figure 1. The image is a summed 40 ks exposure obtained with the ACIS-I3 front-illuminated device and the ACIS-S3 back-illuminated device. The top panel shows the unsmoothed image, after event fil-

[1] Harvard-Smithsonian Center for Astrophysics, 60 Garden Street, Cambridge, MA 02138.
[2] Massachusetts Institute of Technology, Center for Space Research, 70 Vassar Street, Building 37, Cambridge, MA 02139.
[3] Department of Engineering Physics, University of Wollongong, Wollongong, NSW 2522, Australia.
[4] Department of Astronomy, University of Virginia, P.O. Box 3818, Charlottesville, VA 22903-0818.

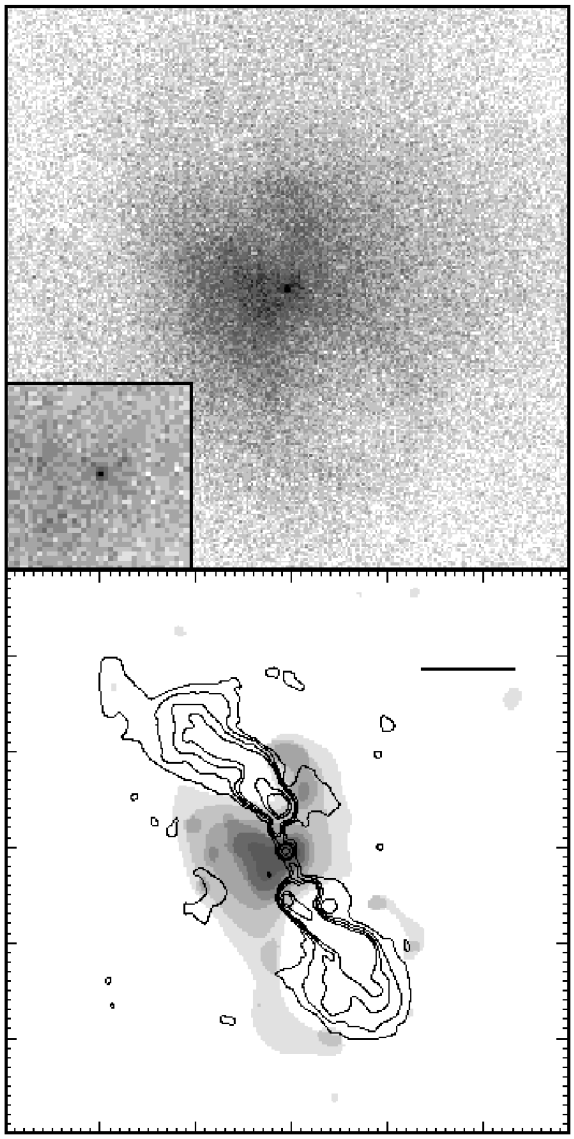

FIG. 1.—*Top*: 40 ks integration X-ray image of the central region of the Hydra A cluster centered on the nuclear X-ray point source (*inset*). *Bottom*: Wavelet-smoothed and reconstructed image of the same region superposed on the 6 cm VLA radio image of Hydra A (*contours*). The scale bar is 20″ in length.

tering, centered on the X-ray point source. The X-ray emission shows a great deal of structure on scales ranging from less than a few kiloparsecs to tens of kiloparsecs that have not been seen in earlier X-ray imagery. An X-ray point source (R.A. = $09^h18^m05^s.77$, decl. = $-12°05'42''.53$, J2000), shown as an inset to the top panel of Figure 1, coincides with the central radio core and BCG nucleus. The bottom panel of Figure 1 shows the wavelet-smoothed X-ray image. The emission is concentrated in a central triangular region, 10″–15″ in size, and in fainter fingers of emission extending northeast and southwest of the center. The emission spectrum of this material is consistent with thermal emission from ~3 keV cluster gas. Two depressions in the X-ray emission, 20″–30″ in diameter, are seen ~20″ to the north and south of the cluster center. The surface brightness within these cavities is a factor of ~1.5 lower than the mean surface brightness of the emission at similar radii from the center. This decline in surface brightness is consistent with these regions being devoid of gas at the ambient temperature and density.

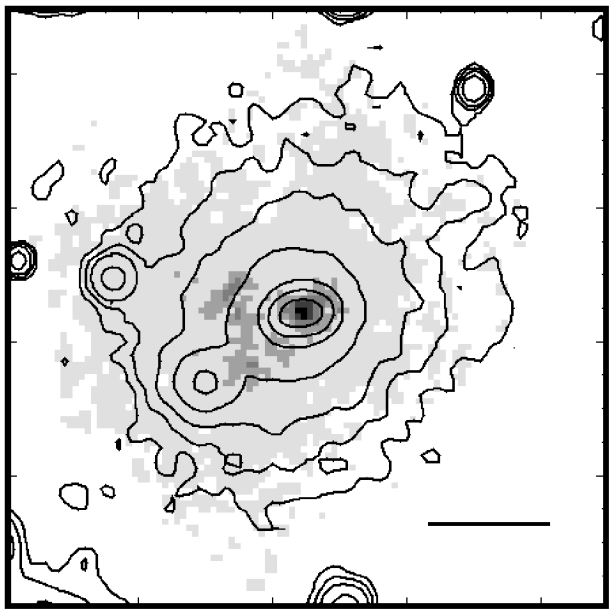

FIG. 2.—Detail of the X-ray emission gray-scale–smoothed with an FWHM = 0.″86 Gaussian and superposed on the *U*-band contours of the BCG (McNamara 1995). The central disk of gas and the young stars are the elliptical contours centered on the X-ray point source. The scale bar is 10″ in length.

2.2. *Radio Morphology*

A 6 cm VLA image obtained in the A array, obtained by G. Taylor, is shown superposed on the wavelet-reconstructed X-ray image in Figure 1. The cavities in the X-ray emission are filled by emission from the radio lobes, and the X-ray cavities and radio lobes are remarkably similar in shape. Similar cavities have been seen in *ROSAT* imagery of the Perseus cluster (Böhringer et al. 1993) and in Cygnus A (Carilli, Perley, & Harris 1994). Heinz, Reynolds, & Begelman (1998) proposed a model to explain such cavities as a shell of shocked gas displaced by the relativistic material from the radio jet. This model would imply that the X-ray emission surrounding the radio source should be considerably hotter than the material away from the radio source. We evaluate this interpretation of the radio cavities, and we explore the physical state of the cluster gas in § 2.4.

2.3. *Optical Morphology: The Central Disk*

Spatial correlations between the X-ray, optical, and radio emission are present in the inner 20 kpc of the BCG. The *U*-band contours are superposed on a gray-scale X-ray image in Figure 2. The X-ray point source is centered on a gaseous disk of nebular emission and young blue stars in rotation about the nucleus (Ekers & Simkin 1983; Baum et al. 1988; McNamara 1995; Hansen et al. 1995; Melnick et al. 1997). The disk of star formation is about 10 × 7 kpc in size, and is roughly 0.7 mag bluer than the $U-I$ color of the galaxy's halo (McNamara 1995). The nebular emission (Baum et al. 1988; Hansen et al. 1995) extends over a similar region.

The brightest X-ray emission, apart from the point source, appears in a flattened structure coincident with the disk, whose ellipticity ranges between 0.3 and 0.4 to a radius of 3″ and in an irregular structure several arcseconds east of the disk. The

X-ray point source is within a half-arcsecond of the radio core (Fig. 1) and the BCG's nucleus. This positional correspondence is within *Chandra*'s absolute pointing error. The surface brightness of the light gray region in Figure 2 is ≃30% fainter than the dark gray structure just east of the disk. This fainter emission forms a wedge-shaped structure that widens toward two companion galaxies projected onto the BCG (see also Fig. 1). The asymmetry in the X-ray structure may be caused, in part, by an irregular potential well associated with a merger between the BCG and the companion galaxies (Ekers & Simkin 1983).

The radio jets (Fig. 1) emerge from the optical disk at roughly a 20° angle from the disk's minor optical axis and rotation axis, and they flare into lobes where the gas pressure reaches $\sim 6 \times 10^{-10}$ ergs cm^{-3}. The jets show no obvious signs of interacting with the optical disk emission or the X-ray emission in the central flattened structure.

2.4. *Physical State of the X-Ray–emitting Gas*

We computed the radial distribution of density, temperature, and pressure of the gas in the central 84 kpc. These parameters were computed by fitting a single-temperature MEKAL model in XSPEC to the X-ray emission in annuli centered on a central X-ray point source. The fluxes were corrected for cluster emission at large radii projected onto the inner regions (deprojected), and the abundance and foreground absorption were free parameters in the models. The abundances were found to be ∼0.4 solar, and the foreground absorption was found to be $\sim 2 \times 10^{20}$ cm^{-2}. No evidence for excess absorption from cold gas within the cluster is found, with the exception of a large column toward the nuclear point source (§ 4). In addition, we constructed hardness ratio profiles $\kappa(R)$ by taking the ratios of the X-ray surface brightnesses I in several passbands. These profiles are plotted in Figure 3. The hardness ratios are defined as $\kappa_1 = I(0.5 \rightarrow 1.5)/I(1.5 \rightarrow 2.5)$ (*open circles*) and $\kappa_2 = I(0.5 \rightarrow 2.5)/I(2.5 \rightarrow 6.0)$ (*filled circles*), where the figures in parentheses are the passbands in units of keV. The spectrum is harder as $\kappa(R)$ decreases. The n_e, kT, and P profiles exclude the central point source, while the hard (absorbed) point source is included in the hardness ratio plot.

The temperature increases from ∼3 keV in the central 10 kpc to ∼4 keV at 80 kpc. The rms density within the central 10 kpc is $n_e = 0.06$ cm^{-3}. The density declines with radius as $\sim r^{-1}$ to a radius of 70 kpc, and the gas pressure declines by a factor of ∼6 from the center to 70 kpc. The central point source is considerably harder than the surrounding emission within a 10 kpc radius. Beyond the central source, κ decreases (hardens) 10%–30% between the center and 80 kpc. The broadband κ_2 shows the larger decline. There is no significant difference between hardness ratio profiles including or excluding the flux from the cavities. Furthermore, the hardness ratio surrounding the radio lobes varies between $\kappa \sim 0.8$ and 1.3, which is consistent with values at similar cluster radii but away from the lobes. There is no evidence for structure in the hardness ratio map associated with the radio lobes, and no evidence for spectral hardening due to shocks.

We note that in the 0.5–7 keV *Chandra* band, the predicted count rate for gas heated by shocks to a temperature as large as 80 keV would be about $\frac{2}{3}$ of that for gas with the same emission measure at a temperature of 5 keV. If gas in or near the cavities had been compressed and heated in a shock, the density enhancement in the shock would more than compensate for the loss of sensitivity due to the temperature rise. The shocked gas within the cavity would then appear roughly a factor of 2.5 brighter than the unshocked ambient gas, which is not observed.

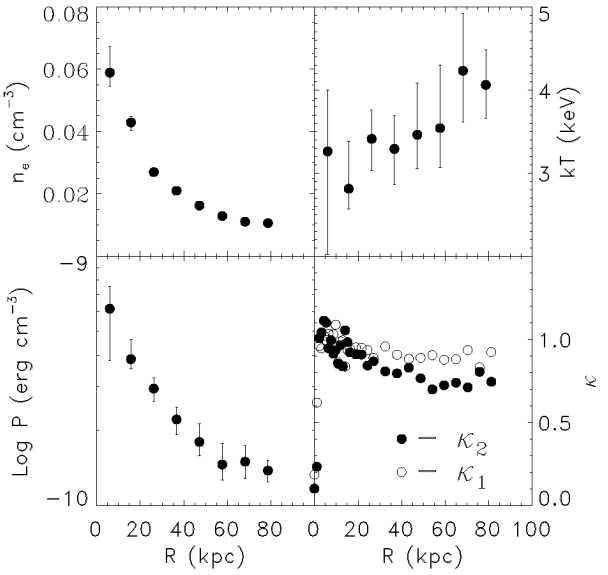

FIG. 3.—Run of electron density (*upper left*), temperature (*upper right*), pressure (*lower left*), and hardness ratio (*lower right*). In this convention, hardness increases as κ decreases.

3. DISCUSSION

3.1. *Origin of the X-Ray Cavities*

There is no indication that the gas surrounding the radio source is hotter than the ambient cluster gas. This behavior is inconsistent with strongly shock-heated gas, as is suggested by the Heinz et al. (1998) model, but is consistent with the cool central material being displaced as the radio source expands subsonically. There is no evidence that the radio source is heating the gas outside the cavities (P. E. J. Nulsen et al. 2000, in preparation).

We now calculate the minimum energy required by the radio source to displace the gas using the southern cavity for illustration. The center of the southern cavity is approximately 26″ from the X-ray nuclear point source. The electron density in the annulus centered on the southern cavity is $n_e = 0.027$ cm^{-3}, and the temperature is $kT = 3.4$ keV, giving a pressure $p = 2.8 \times 10^{-10}$ ergs cm^{-3}. Based on the deprojection, undisturbed gas in a volume the size of this cavity would have contributed about 2000 counts. This is consistent with our estimate for the count deficit in the cavity. We therefore assume that the ambient intracluster medium has been displaced from this region by the radio source. Since there is no spectral hardening at the edges of the cavities, we assume that the pressure within them is similar to the ambient gas pressure.

The minimum energy required to push the gas out of a sphere of radius 15 kpc is then $pV \simeq 1.2 \times 10^{59}$ ergs. Since there are no signs of shocks, we assume that gas motions are subsonic and can be ignored, so that the total energy required to inflate the cavity is a modest multiple of this.

The cavity would take $\sim 2 \times 10^7$ yr to expand at approximately the sound speed. The cavity is also buoyant, so it must be refilled on a similar timescale, $\simeq 2R[r/GM(R)]^{1/2}$, where r is the radius of the cavity and R is the distance to the cluster center. From the deprojection, a rough estimate of the total gravitating mass within 30 kpc of the cluster center is

$M(R) = 3 \times 10^{12}\ M_\odot$, giving a refilling time of about 6×10^7 yr. Thus, the minimum mechanical power from the southern radio jet required to maintain the cavity is $\sim 6 \times 10^{43}$ ergs s^{-1}, which is comparable to the total radio power from Hydra A (Ekers & Simkin 1983). Either timescale implies an efficiency of conversion of kinetic energy to radio power of order unity, and we need not postulate the existence of kinetic luminosity substantially in excess of the luminous radio power (e.g., Heinz et al. 1998).

Our interpretation requires the radio lobes and surrounding gas to be nearly in pressure equilibrium. However, the gas pressure appears to be more than an order of magnitude larger than the minimum-energy pressure of the radio lobes (Taylor et al. 1990). If the lobes are in pressure balance with the cluster gas and if equipartition between the magnetic field and relativistic particles is to be maintained, then one or more of the following conditions is implied. There is a significant additional contribution to the particle energy density from low-energy electrons or from protons (e.g., Böhringer et al. 1993); the radio plasma filling factor is significantly less than 1, or the radio lobes are at significantly larger radii in the cluster atmosphere than their projected positions.

3.2. *The Cooling Flow*

Gas with the observed central density $n_e(r < 10\ \mathrm{kpc}) = 0.06\ \mathrm{cm}^{-3}$, temperature $kT = 3$ keV, and abundance of 0.4 solar has a radiative cooling time of $\sim 6 \times 10^8$ yr. If such cool material has been present in the cluster for $\gtrsim 1$ Gyr, the gas should cool to low temperatures and flow to the center of the cluster. The *Chandra* data allow us to obtain high-quality spectra of several independent regions within the central 80 kpc of the cluster. We have fitted an absorbed thermal (MEKAL) plus constant pressure cooling-flow (MKCFLOW) model to a series of eight circular apertures ranging in equal steps from 10″ to 80″ in radius. The central 1.″5 was excluded. Assuming spherical symmetry, we attribute the differences in mass deposition rate M for successive apertures to the annulus they define, apply a standard geometric deprojection to convert these to mass deposition rates per unit volume, and calculate total M's for the spheres. The total mass deposition rate within a 74 kpc sphere is $34 \pm 5\ M_\odot\ \mathrm{yr}^{-1}$, and $M(R) \sim R^{1.1}$. We interpret this result with caution. Although a cooling-flow model provides a good fit to the data, a single-temperature model at each radius beyond 10 kpc would adequately describe the data given the uncertainty in the current ACIS calibration.

3.3. *Cooling Rate versus Star Formation Rate*

The most controversial issue concerning cooling flows is the fate of the cooling material. We now ask whether or not the accretion rates derived from the new X-ray data are consistent with the star formation rate. Star formation appears to be confined to the disk (§ 2.3), whose young stellar population mass estimate ranges from $10^{7.7}$ to $10^9\ M_\odot$ (McNamara 1995; Hansen et al. 1995). Estimates of the average star formation rates vary from $\lesssim 1\ M_\odot\ \mathrm{yr}^{-1}$ for continuous star formation for ~ 1 Gyr duration to $\sim 15\ M_\odot\ \mathrm{yr}^{-1}$ for a younger, $\sim 10^8$ yr old burst population. The degree to which star formation may be consuming the cooling gas depends on factors that include the relative ages of the cooling flow and the stellar population and the stellar initial mass function. In the central 10 kpc, a region somewhat larger than the central optical disk, the mass deposition rate is $4 \pm 2\ M_\odot\ \mathrm{yr}^{-1}$. Thus, the observed rates of star formation can account entirely for the mass cooling within this region, regardless of the age of the cooling flow. However, the disk star formation would provide a sink for the cooling gas within the entire 74 kpc region for $\lesssim 3 \times 10^6$ yr, which is much smaller than the minimum time of ~ 1 Gyr required to establish a cooling flow. If material is indeed cooling to low temperatures at larger radii, it remains unaccounted for. However, we find no evidence that the radio source is heating the gas and reducing the cooling rates.

4. THE CENTRAL POINT SOURCE

We extracted the spectrum of the central point source within a 1″ radius aperture. The background was taken from the annular region between $r = 1''$ and 2.″5 centered on the point source. The net point-source spectrum was found by subtracting the background spectrum, after normalizing by the relative areas of the central and annular regions. The net spectrum appears to be a power law absorbed by an $N_{\mathrm{H}} = 4.5(2.2\text{–}9.9) \times 10^{22}\ \mathrm{cm}^{-2}$ (90% errors). The point-source flux, uncorrected for absorption, is $f(0.6\text{–}6.0) = 1.0 \times 10^{-13}$ ergs s^{-1} cm^{-2}, which corresponds to a luminosity of 6.9×10^{41} ergs s^{-1}. The absorbing column toward the point source is more than 2 orders of magnitude larger than the Galactic foreground column and is confined to a spatial extent of less than 1.″5.

This column density is in reasonably good agreement with the column of neutral hydrogen absorption seen toward the VLBI radio source in the nucleus of the galaxy (Taylor 1996). The radio absorption map confines the spatial extent of this high column density material to a region of $\lesssim 24$ pc in the nucleus of the galaxy. Assuming that the X-ray and radio flux is absorbed by the same material, the combined observations restrict the X-ray–emitting region of the point source to $\lesssim 24$ pc.

P. E. J. N. gratefully acknowledges the hospitality of the Harvard-Smithsonian Center for Astrophysics. B. R. M. acknowledges grant NAS8-39073. We thank the referee, Keith Arnaud, for constructive comments.

REFERENCES

Baum, S. A., Heckman, T., Bridle, A., van Breugel, W., & Miley, G. 1988, ApJS, 68, 643
Böhringer, H., Voges, W., Fabian, A. C., Edge, A. C., & Neumann, D. M. 1993, MNRAS, 264, L25
Carilli, C. L., Perley, R. A., & Harris, D. E. 1994, MNRAS, 270, 173
David, L. P., Arnaud, K. A., Forman, W., & Jones, C. 1990, ApJ, 356, 32
Dwarakanath, K. S., Owen, F. N., & van Gorkom, J. H. 1995, ApJ, 442, L1
Ekers, R. D., & Simkin, S. M. 1983, ApJ, 265, 85
Hansen, L., Jørgenson, H. E., & Nørgaard-Nielson, H. U. 1995, A&A, 297, 13
Heinz, S., Reynolds, C. S., & Begelman, M. C. 1998, ApJ, 501, 126
Ikebe, Y., et al. 1997, ApJ, 481, 660
McNamara, B. R. 1995, ApJ, 443, 77
Melnick, J., Gopal-Krishna, & Terlevich, R. 1997, A&A, 318, 337
Peres, C. B., Fabian, A. C., Edge, A. C., Allen, S. W., Johnstone, R. M., & White, D. A. 1998, MNRAS, 298, 416
Taylor, G. B. 1996, ApJ, 470, 394
Taylor, G. B., Perley, R. A., Inoue, M., Kato, T., Tabara, H., & Aizu, K. 1990, ApJ, 360, 41
White, D. A., Jones, C., & Forman, W. 1997, MNRAS, 292, 419